Available online at www.sciencedirect.com
SCIENCE DIRECT®
PERGAMON
Polyhedron 22 (2003) 2415–2422
POLYHEDRON
www.elsevier.com/locate/poly

Molecular compounds based on DT-TTF and $Au(cdc)_2$ complex. Structural, magnetic and electrical properties

Xavi Ribas [a], Marta Mas-Torrent [a], Concepció Rovira [a,*], Jaume Veciana [a], João C. Dias [b], Helena Alves [b], Elsa B. Lopes [b], Manuel Almeida [b], Klaus Wurst [c]

[a] *Institut de Ciència de Materials de Barcelona, CSIC, Campus de la UAB, E-08193 Bellaterra, Spain*
[b] *Departamento de Química, Instituto Tecnológico e Nuclear, P-2686-953 Sacavem, Portugal*
[c] *Institut für Allgemeine Anorganische und Theoretische Chemie, Universiat Innsbruck, Innrain 52a, Innsbruck, Austria*

Received 24 October 2002; accepted 3 January 2003

Abstract

The synthesis and characterisation of two new radical ion salts based on the donor dithiophenetetrathiafulvalene (DT-TTF) and the anion $Au(cdc)_2^-$ (cdc = cynanodithioimido carbonate) are described. These salts were characterised as the mixed valence compound $(DT\text{-}TTF)_2(Au(cdc)_2)$ (**1**) and the completely ionic salt $(DT\text{-}TTF)(Au(cdc)_2)$ (**2**). The X-ray crystal structure of both compounds show that they are formed by chains of donor molecules separated by anions, but, whereas in compound **2** the donors form uniform stacks, in compound **1** they are dimerised. The electrical conductivity measured in a single crystal at room temperature is 0.2 S cm^{-1} for **1** and 1.7×10^{-2} S cm^{-1} for **2**, both revealing semiconducting behaviour. Magnetic measurements indicate strong antiferromagnetic interactions between the donors in compound **2**, and a possible spin-Peierls transition at low temperature for compound **1**.

Keywords: Tetrathiafulvalenes; Metal bis-dithiolene complexes; Magnetism; Electrical conductivity; X-ray crystal structures

1. Introduction

Recent studies have reported new charge-transfer compounds based on dithiophenetetrathiafulvalene (DT-TTF) and transition metal bis-dithiolene complexes which, when having the diamagnetic counterion $Au(mnt)_2$, show a spin-ladder magnetic behaviour [1]. Spin-ladders, especially even-leg ladders, are very interesting since it has been demonstrated that they have only short-range order and a finite spin gap [2]. In addition, holes injected into even-leg ladders are predicted to pair and possibly show superconductivity. The intriguing properties of spin-ladders prompted us to pursue the research in this field and the study of related compounds with similar properties.

Aiming at the preparation of new molecular compounds with a spin-ladder magnetic behaviour similar to that of $(DT\text{-}TTF)_2(Au(mnt)_2)$ [1b], we selected the gold complex $Au(cdc)_2$ (cdc = cynanodithioimidocarbonate) (see Scheme 1), with similar dimensions but of lower symmetry, to be combined with the same donor DT-TTF [3]. Despite the similarities between the acceptor complexes $Au(mnt)_2$ and $Au(cdc)_2$, the combination of the latter with DT-TTF does not give any compound with the suitable arrangement of the donor molecules in the crystal for having a spin-ladder behaviour. Depending on the electrocrystallisation conditions (solvent and current density), two different salts have been found for this system: a mixed-valence molecular compound $(DT\text{-}TTF)_2(Au(cdc)_2)$ (**1**) and a radical ion salt with com-

* Corresponding author. Tel.: +34-93-580-1853; fax: +34-93-580-5729.
E-mail address: cun@icmab.es (C. Rovira).

0277-5387/03/$ - see front matter
doi:10.1016/S0277-5387(03)00255-9

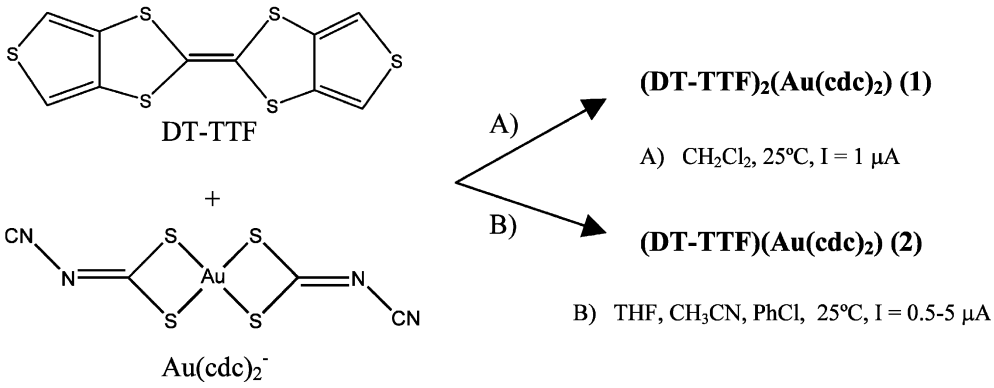

Scheme 1.

pletely ionic character (DT-TTF)(Au(cdc)$_2$) (**2**). In this paper, we describe the synthesis and crystal structure of compounds **1** and **2** as well as their characterisation by magnetic susceptibility, EPR and electrical transport measurements.

2. Experimental

2.1. Synthesis

The DT-TTF donor ($\Delta^{2,2'}$-bithieno[3,4-d]-1,3-dithiol) was synthesised the following methods described in the literature [3]. The cdc ligand was obtained as a dipotassium salt, K_2(cdc)$_2$, using a synthesis route previously reported [4]. The gold complex (nBu$_4$N)[Au(cdc)$_2$], was obtained from this ligand salt and $HAuCl_4 \cdot 3H_2O$, following a general procedure previously described [5]. Prior to its use (nBu$_4$N)[Au(cdc)$_2$] was recrystallised from methanol.

Salts **1** and **2** were obtained by electrocrystallisation in conventional H-shaped electrochemical cells with Pt electrodes. The [Au^{III}(cdc)$_2$](nBu$_4$N) complex (3.2 mg, 4.77×10^{-6} mol) was dissolved with 12 ml of the desired solvent previously dried and degassed with Ar. Then 6 ml of the complex solution were used to dissolve 3 mg (9.48×10^{-6} mol) of DT-TTF and placed in the anodic side of the cell. The cathodic compartment was filled with the remaining 6 ml of the gold complex solution. The cell compartments were purged with Ar before the Pt-wire electrodes were introduced and the system was sealed with the appropriate caps. Galvanostatic conditions were maintained and the crystals grown on the anode were collected after about 7 days, by filtering the solution and washing with fresh solvent.

Compounds **1** or **2** were obtained depending on the solvents and current densities used. (DT-TTF)$_2$(Au(cdc)$_2$) (**1**) was obtained as small ($0.2 \times 0.15 \times 0.05$ mm^3) black plate shaped crystals suitable for X-ray diffraction studies, using CH_2Cl_2 as a solvent, and a current of 1 μA. (UV/Vis (KBr pellet): λ_{max} (nm) = 690, 3000 ('A' band); IR (KBr pellet): ν (cm^{-1}) = 3087, 2922, 2184, 1473, 1342, 1258, 1102, 840, 776, 700, 568, 509).

(DT-TTF)(Au(cdc)$_2$) (**2**) was obtained under a wide range of experimental conditions; either THF, CH_3CN or PhCl can be used as solvent and currents in the range of $I = 0.5$–5 μA. Compound **2** was also obtained in CH_2Cl_2 at a constant current of 5 μA. (UV/Vis (KBr pellet): λ_{max} (nm) = 620, no 'A' band; IR (KBr pellet): ν (cm^{-1}) = 3095, 2925, 2193, 1496, 1394, 1339, 1295, 1105, 1020, 958, 899, 847, 782, 561, 483).

2.2. Physical measurements

IR spectra (7000–400 cm^{-1}) were recorded in a Perkin–Elmer Spectrum One model infrared spectrophotometer and the electronic spectra were recorded in a Varian Cary 5 UV–Vis–NIR spectrophotometer (250–3000 nm).

The electrical resistivity was measured along the long axis of selected single crystals placed in a cell attached to the cold stage of a close-cycle helium refrigerator. Thin $\phi = 25$ μm gold wires were directly attached to the sample with platinum paint to achieve a four-in-line contact geometry and measurements were made applying an AC current of 1 μA at 77 Hz, the voltage being measured by a lock-in amplifier (EG&G Par 5316) [6,7]. The samples were previously checked for unnested/nested voltage ratio [8] which was kept below 5%.

EPR spectra were obtained in a conventional X-band spectrometer (Bruker ESP 300 E) equipped with a microwave bridge ER041XK, a rectangular cavity operating in T102 mode, a field controller ER 032M system and a Oxford ESR-900 cryostat, which enabled measurements in the temperature range 110–350 K and the temperature was monitored by a Au(0.07 at. % Fe)-chromel thermocouple placed close to the sample. The measurements were performed on single crystals, placed inside a quartz tube. The modulation amplitude was kept well below the line width and the microwave power well below saturation.

The static magnetic susceptibility of polycrystalline samples, was measured in the temperature range 2–300 K using a Faraday system (Oxford Instruments) equipped with a 7 T superconducting magnet. The measurements were performed under a static magnetic field of 5 T. The force on the samples, contained in a previously measured thin-walled Teflon bucket, was measured with a microbalance (Sartorius S3D-V) applying forward and reverse gradients of 1 T m^{-1}. The paramagnetic susceptibility was calculated considering a diamagnetic correction, estimated from tabulated Pascal constants.

2.3. Structure determination

Suitable crystals of **1** and **2** were used for X-ray diffraction data collection on a Nonius Kappa CCD with graphite-monochromatized Mo Kα-radiation ($\lambda = 0.71073$ Å) and a nominal crystal to area detector distance of 36 mm. The relevant crystal data are summarised in Table 1. Intensities were integrated using DENZO and scaled with SCALEPACK. Several scans in ϕ and ω direction were made to increase the number of redundant reflections, which were averaged in the refinement cycles. This procedure replaces an empirical absorption correction. The structure was solved with direct methods SHELXS-86 and refined against F^2 SHELX-97. Hydrogen atoms at carbon atoms were added geometrically and refined using a riding model. All non-hydrogen atoms were refined with anisotropic displacement parameters.

Table 1
Crystal data and structural refinement parameters for **1** and **2**

	$(DT\text{-}TTF)_2Au(cdc)_2$ (**1**)	$(DT\text{-}TTF)Au(cdc)_2$ (**2**)
Empirical formula	$C_{24}H_8S_{16}N_4Au$	$C_{14}H_4S_{10}N_4Au$
Formula weight	1062.27	745.48
Temperature (K)	228(2)	233(2)
Wavelength (Å)	0.71073	0.71073
Crystal system	triclinic	monoclinic
Space group	$P\bar{1}$ (No. 2)	$C2/c$
a (Å)	8.192 (1)	23.546(2)
b (Å)	8.530 (2)	3.8283(9)
c (Å)	12.728 (2)	25.173(2)
α (°)	77.47 (1)	90.00
β (°)	71.83 (1)	115.892(4)
γ (°)	74.99(1)	90.00
V (Å^3)	807.2(2)	2041.3(5)
Z	1	4
D_{calc} (g cm^{-3})	2.185	2.427
μ (mm^{-1})	5.621	8.242
Crystal size (mm)	$0.2 \times 0.15 \times 0.05$	$0.35 \times 0.03 \times 0.02$
Index ranges	$0 \le h \le 8$ $-7 \le k \le 8$ $-11 \le l \le 12$	$0 \le h \le 25$ $-4 \le k \le -4$ $-27 \le l \le 24$
Reflections collected	2649	4345
Independent reflections	1500	1413
Number of parameters	206	133
Reflections $> 2\sigma(I)$	1432	1159
R_1 [a]	0.0333	0.0247
wR_2 [b]	0.0851	0.0446

[a] $R_1 = \Sigma|F_o - F_c|/\Sigma F_o$.

[b] $wR_2 = \{\Sigma[w(F_o^2 - F_c^2)^2]/\Sigma[w(F_o^2)^2]\}^{1/2}$ where $w = 1/[\sigma^2(F_o^2 + (aP)^2 + bP]$, $P = (F_o^2 + 2F_c^2)/3$, and a and b are constants given in the supporting information.

3. Results and discussion

3.1. Synthesis of *1* and *2*

The electrocrystallisation reaction by oxidation of the donor DT-TTF in the presence of the $[Au(cdc)_2]TBA$ complex affords different crystalline compounds **1** and **2** depending on the experimental conditions used (Scheme 1). In fact, the mixed-valence compound $(DT\text{-}TTF)_2(Au(cdc)_2)$ (**1**) was obtained only when CH_2Cl_2 as a solvent and a constant current of 1 μA were used. On the other hand, the completely ionic salt $(DT\text{-}TTF)(Au(cdc)_2)$ (**2**) was obtained using CH_3CN, THF, or PhCl as solvents with current intensities ranging from 0.5 to 5 μA, and even when CH_2Cl_2 was used with a high current of 5 μA. In all the experiments the concentration of DT-TTF was 7.90×10^{-4} M and the molar ratio DT-TTF/$Au(cdc)_2 \approx 2$. These results indicate that the thermodynamically more stable salt is the radical ion salt $(DT\text{-}TTF)(Au(cdc)_2)$ (**2**).

A characteristic mixed-valence 'A' band is observed, centred at 3000 cm^{-1}, for **1** and is absent in the IR and UV–Vis–NIR spectra of **2** in accordance with the mixed valence character of salt **1** and the completely ionic one of salt **2**.

3.2. Description of crystal structures

Compound **1** crystallises in the triclinic $P\bar{1}$ system (Table 1) and the asymmetric unit comprises one DT-TTF donor unit and one half of the Au complex anion with the metal in an inversion centre (Fig. 1(A)). Selected bond distances and angles are listed in Table 2. Au–S bond distances are ~2.33 Å, similar to those previously found in other monoanionic gold bis-dithiolate complexes [1a]. The crystal packing of $(DT\text{-}TTF)_2[Au(cdc)_2]$ (see Fig. 2) consists of stacks of the DT-TTF units along [1 1 0] axis and $Au(cdc)_2$ anions which are almost perpendicular to the donors. This crystal structure is similar to that of the $(TTDM)_2[Au(mnt)_2]$ salt [9]. The donor stacks are arranged in layers parallel to the ab plane sustained by two S···S contacts of 3.522 and 3.858 Å, connecting the ends of DT-TTF molecules in neighbouring stacks. The donor layers alternate with layers of $Au(cdc)_2$ anions

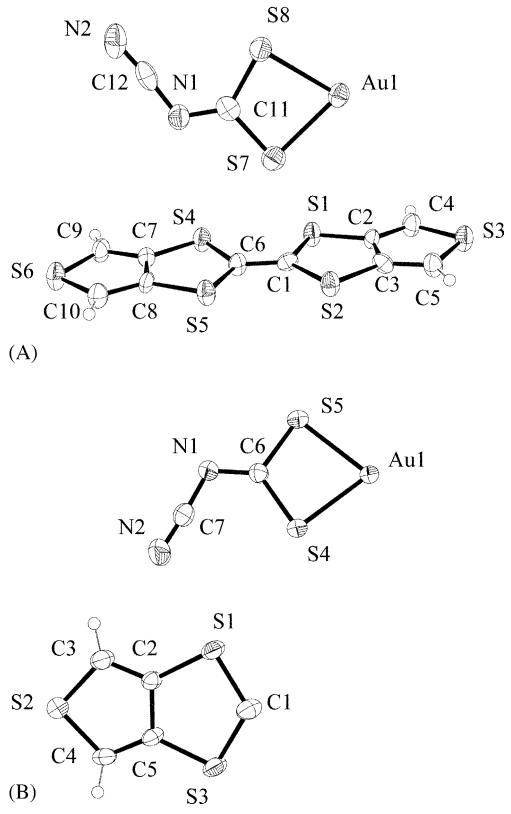

Fig. 1. ORTEP plot of the asymmetric units of (A) (DT-TTF)$_2$[Au(cdc)$_2$] (**1**) and (B) (DT-TTF)[Au(cdc)$_2$] (**2**).

along [0 $\bar{1}$ 1]. The donor molecules are dimerised showing very small interactions between them inside the stack. There are intra-dimer and inter-dimer S···S contacts of 3.690 and 4.088 Å, respectively (see Fig. 3). There are also several N···H–C hydrogen bonds, S···C and S···N contacts between donors and acceptors which are summarised in Table 2.

The (DT-TTF)(Au(cdc)$_2$) salt **2** crystallises in the monoclinic space group $C2/c$ with $z = 4$ (Table 1). The asymmetric unit comprises one half of the DT-TTF donor unit and one half of the Au complex anion (Fig. 1(B)). Selected bond distances and angles are listed in Table 3. As shown in Fig. 4 the crystal structure consists of segregated uniform stacks of DT-TTF$^{+\bullet}$ radical-cations and Au(cdc)$_2^-$ anions both along the b axis. The donor molecules are stacked almost perpendicularly to the stacking axis b with an interplanar distance of 3.697 Å, while the anions are tilted (their normal forms an angle of 25° with b). Each DT-TTF$^{+\bullet}$ radical-cation establishes short S···S contacts and hydrogen bonds with six molecules of the surrounding gold complexes (see Fig. 5), and four S···S contact (3.945 Å) with DT-TTF$^{+\bullet}$ molecules in neighbouring stacks. Similarly, each Au(cdc)$_2^-$ is surrounded by six DT-TTF$^{+\bullet}$ molecules providing short intermolecular contacts (see Table 3).

Table 2
Selected bond lengths (Å), angles (°) and intermolecular contacts for (DT-TTF)$_2$[Au(cdc)$_2$] (**1**)

Au1–S7	2.323(3)	C6–S4	1.752(8)
Au1–S8	.336(2)	C6–S5	1.736(9)
N1–C11	1.282(12)	C2–C3	1.428(12)
N2–C12	1.168(14)	C7–C8	1.416(12)
N1–C12	1.325(15)	S3–C4	1.701(10)
C1–C6	1.361(12)	S3–C5	1.704(9)
C1–S1	1.741(9)	S6–C9	1.715(9)
C1–S2	1.758(9)	S6–C10	1.696(10)
S7–Au1–S7′	180.0	C6–C1–S1	120.7(7)
S8–Au1–S8′	180.0	C6–C1–S2	122.0(7)
S7–Au1–S8	75.33(9)	S1–C1–S2	117.1(5)
S7–Au1–S8′	104.67(9)	S4–C6–S5	117.1(5)
C11–N1–C12	117.2(8)	S1–C1–C6–S4	0.3
C1–C6–S4	119.5(7)	S1–C1–C6–S5	−178.7
C1–C6–S5	123.4(7)	S2–C1–C6–S4	176.0
		S2–C1–C6–S5	−3.0
Contacts			
Intra-dimer		Au(cdc)$_2$···DT-TTF	
6 × (S···S)	3.674	1 × (S···H–C)	2.885
2 × (S···S)	3.690	1 × (N···H–C)	2.489
2 × (S···S)	3.860	1 × (C···S)	3.479
Inter-dimers		1 × (S···C)	3.417
2 × (S···S)	4.088	1 × (S···C)	3.321
C···C	3.916	1 × (N···S)	3.271
S···H–C	3.471		
Inter DT-TTF's			
2 × (S···S)	3.522		
2 × (S···S)	3.858		

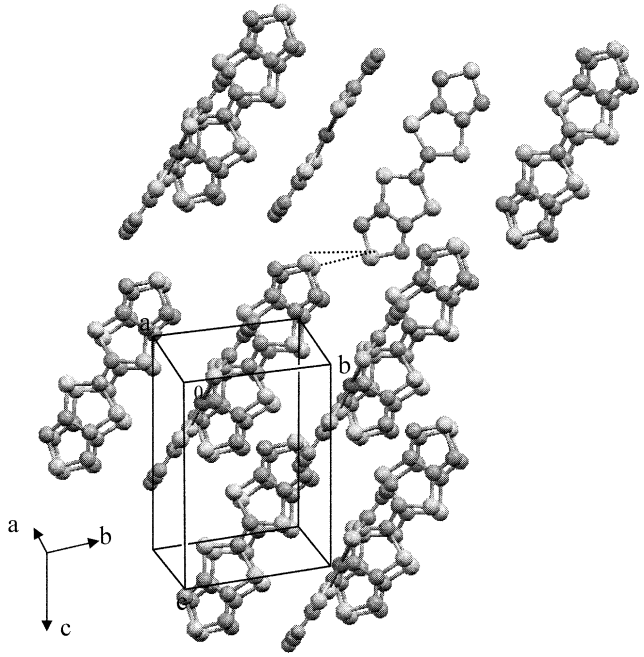

Fig. 2. View of (DT-TTF)$_2$[Au(cdc)$_2$] (**1**) crystal structure. Dotted lines indicate inter-stack S · · · S short contacts.

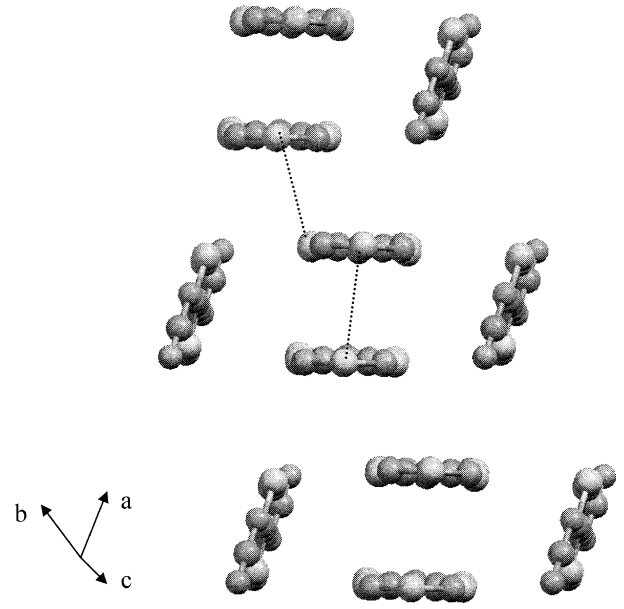

Fig. 3. View of DT-TTF stacks in the crystal structure of **1**. Dotted lines indicate intra and inter-dimer S · · · S contacts along the stacking axis.

Table 3
Selected bond lengths (Å), angles (°) and intermolecular contacts for (DT-TTF)[Au(cdc)$_2$] (**2**)

Au1–S4	2.3310(15)	C1–S1	1.733(6)
Au1–S5	2.3339(15)	C1–S3	1.723(6)
N1–C6	1.291(7)	C2–C5	1.431(8)
N2–C7	1.163(8)	S2–C3	1.698(6)
N1–C7	1.330(9)	S2–C4	1.713(6)
C1–C1′	1.396(12)		
S4–Au1–S4′	180.0	C1′–C1–S1	120.0(6)
S5–Au1–S5′	180.0	C1′–C1–S3	122.1(6)
S4–Au1–S5	75.41(5)	S1–C1–S3	117.9(3)
S4–Au1–S5′	104.59(5)	S1–C1–C1′–S1′	180.0
C6–N1–C7	115.3(5)	S1–C1–C1′–S3′	0.5(9)
Contacts			
		Au(cdc)$_2$···DT-TTF	
Intra stack DT-TTF′s		1 × (S···S)	3.504
6 × (S···S)	3.828	1 × (S···S)	3.554
		2 × (S···H–C)	2.972
Inter stack DT-TTF′s		2 × (S···H–C)	2.993
4 × (S···S)	3.945	2 × (N···H–C)	2.492
		2 × (N···S)	2.932
		2 × (N···S)	3.238

3.3. Electrical transport measurements

The electrical conductivities of **1** and **2** measured in single crystals in the range 140–360 K are shown in Fig. 6. At room temperature compounds **1** and **2** present values of σ (300 K) = 0.2 and 0.017 S cm^{-1} respectively, both displaying a semiconducting behaviour. While **1** presents an almost temperature independent activation energy of ~0.10 eV, compound **2** has a comparable activation energy at room temperature but it shows a rounded maximum in the derivative d ln σ/d(1/T) at ~220 k (see inset of Fig. 6) suggesting a possible gradual transition with a gap increase at this temperature.

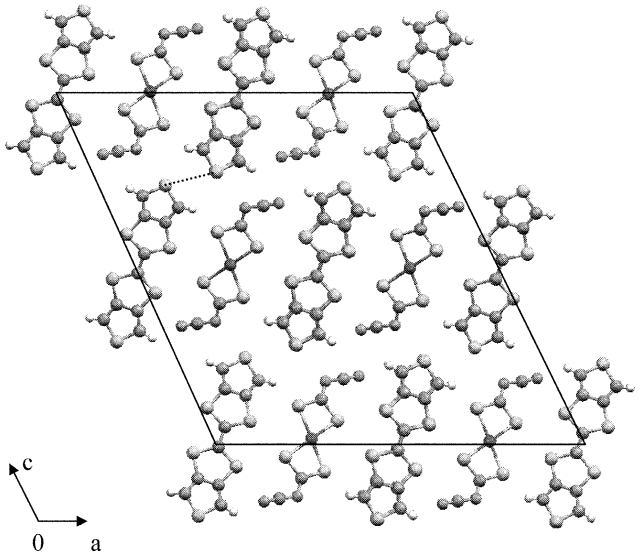

Fig. 4. View of (DT-TTF)[Au(cdc)$_2$] (**2**) crystal structure along ***b***. Botted lines indicate inter-stack S · · · S short contacts.

The observed semiconducting behaviours of these compounds are not unexpected in view of their crystal structures.

The full ionic character of compound **2** and the regular stacking of the donor units lead to a half filled band system, which in narrow band molecular systems invariably is associated with a Mott–Hubbard insulating regime, in agreement with the low conductivity observed for this compound.

Compound **1** as a mixed valence solid with average donor oxidation of (DT-TTF)$^{0.5+}$, would lead to a 3/4 filled band in case of regular stacking. However, the presence of dimerisation in the donors stacks opens a gap in the middle of such band, which becomes effectively 1/2 filled. This situation is comparable to that of (TTDM-TTF)$_2$(Au(mnt)$_2$) with a similar type of crystal packing presenting σ_{RT} = 0.5 S cm^{-1} and an activation energy of E_a = 0.078 eV [9]. The main difference is that in **1** there is a stronger dimerisation of the donor stacks. Also important is the more extended nature of the DT-TTF HOMO with respect to the one of TTDM-TTF as it is expected to lead by inter-stacks contacts to more bidimensional electronic interactions, at variance with (TTDM-TTF)$_2$(Au(mnt)$_2$) which was considered to be an extreme 1D system.

3.4. Magnetic measurements

Single crystal EPR spectra have been registered for compounds **1** and **2**. The g-values found and their

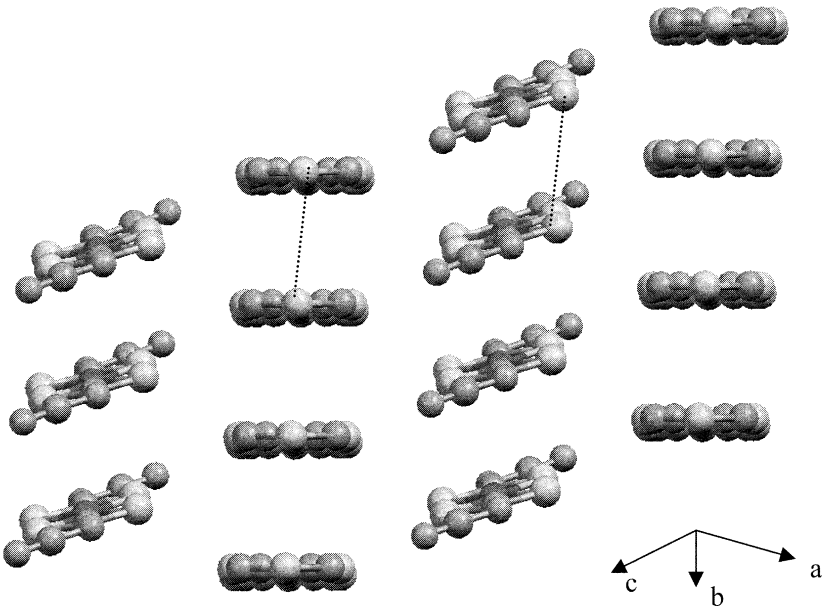

Fig. 5. Partial view of crystal structure of **2** showing side by side DT-TTF+ and $Au(cdc)_2^-$ stacks. The dotted lines indicate S · · · S contacts along the stacking axis.

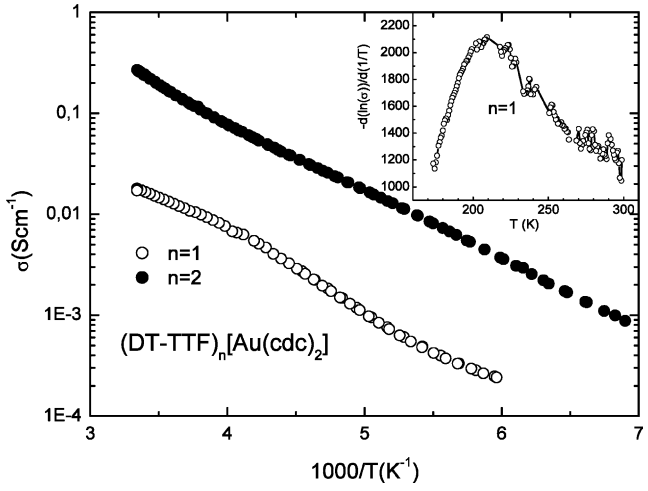

Fig. 6. Single crystal electrical conductivity (σ) of **1** (black circles and **2** (open circles), plotted as σ as a function of the reciprocal temperature, 1/T. The inset shows the derivative $-\mathrm{d}\ln\sigma/\mathrm{d}(1/T)$ of **2** as a function of the temperature.

Table 4
EPR parameters at room temperature for single crystals of **1** and **2**

	g_{max}	g_{inter}	g_{min}
$(DT\text{-}TTF)_2(Au(cdc)_2)$ **(1)**			
g	2.0123	2.0069	2.0013
ΔHpp (G)	7.20	5.67	5.87
$(DT\text{-}TTF)(Au(cdc)_2)$**(2)**			
g	2.0142	2.0069	2.0048
ΔHpp (G)	1.60	1.45	1.76

anisotropy for three different orientations of the crystals relatively to the magnetic field (see Table 4) are typical of the TTF radical-cations, consistent with the presence of diamagnetic monoanionic $Au(cdc)_2$ complexes. It is worth mentioning the significantly narrower line width (ΔHpp) of **2**.

Bulk polycrystalline samples were used to measure the static magnetic susceptibility (χ_p) versus temperature for **1** and **2** in a Faraday balance (Fig. 7). The paramagnetic susceptibility was calculated from raw data considering a diamagnetic correction, estimated from tabulated Pascal constants as 3.73×10^{-4} emu mol^{-1} for **1** and 2.34×10^{-4} emu mol^{-1} for **2**.

For complex **1** the paramagnetic susceptibility χ_p is of the order of 6×10^{-4} emu mol^{-1} at room temperature, and it presents only a small increase upon cooling down to 20 K. Below this temperature χ_p increases and becomes dominated by a Curie tail corresponding to approximately 1% of $S = 1/2$ spins. The intrinsic susceptibility of this compound can be estimated considering this Curie tail (continuous line in Fig. 7) and the result, with a round maximum at ~ 60 K, followed by a sharp decrease of χ_p at 6 K towards zero, suggest a possible spin-Peierls transition at 6 K in a behaviour similar to that of the isostructural compound $(TTDM\text{-}TTF)_2Au(mnt)_2$ [9] or other similar spin-Peierls systems with related 1D structures such as $(TMTTF)_2PF_6$ [10], or $(BCPTTF)_2X$ [11].

Compound **2** exhibits a rather small susceptibility of only $\sim 2 \times 10^{-4}$ emu mol^{-1} at room temperature which further decreases upon cooling. A faster decrease of susceptibility is seen around 220 K, the same temperature range were conductivity data indicated a

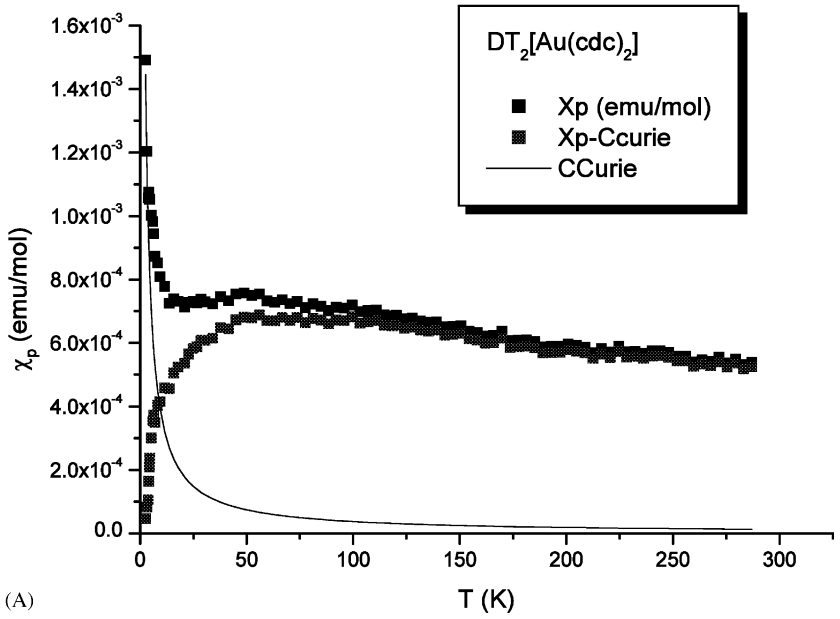

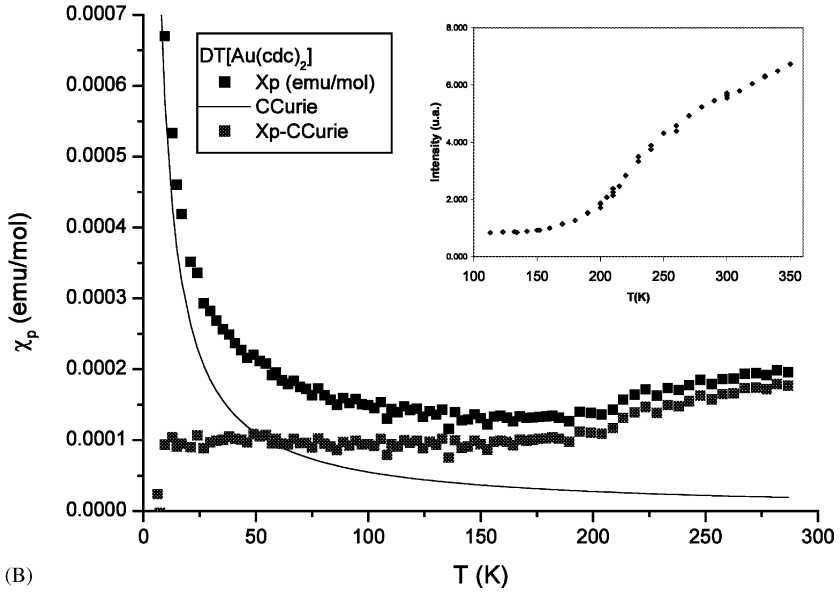

Fig. 7. Temperature dependence of the paramagnetic susceptibility of polycrystalline samples of compounds **1** (A) and **2** (B). Inset shows the EPR signal intensity as a function of temperature of **2**.

change in activation energy. EPR signal intensity measured in the temperature range 110–350 K follows a temperature dependence similar to that of the static susceptibility measurements with a fast decrease of the spin susceptibility around 220 K (Inset Fig. 7(b)). Additional structural characterisation studies of the compound at temperatures below this temperature range are necessary to further enlighten this transition.

The observed magnetic behaviour indicates strong antiferromagnetic coupling between spins in stacked DT-TTF$^{+\bullet}$ units. However, since some transition occurs around 220 K a 1D antiferromagnetic Heisenberg chain model, consistent with the X-ray structure at high temperature can not be used to adjust the data.

4. Conclusions

Two crystal phases have been obtained by combining the DT-TTF donor and the gold complex $Au(cdc)_2^-$. The mixed-valence salt $(DT\text{-}TTF)_2(Au(cdc)_2)$ (**1**), probably the thermodynamically disfavoured phase, is obtained in more restricted conditions of the electrocrystallisation, whether the completely ionic salt

(DT-TTF)(Au(cdc)$_2$) (**2**) is obtained in a wide range of experimental conditions.

Both compounds show structures having stacks of the DT-TTF molecules. However, while in salt **2** fully ionic DT-TTF$^{+\bullet}$ units form regular stacks separated by regular stacks of anions, in compound **1** the partially oxidised DT-TTF$^{+0.5}$ molecules are arranged as dimerised stacks separated by perpendicular anions. Both compounds are semiconductors being the room temperature electrical conductivity value one order of magnitude higher for salt **1**. Magnetic behaviour of **1** indicates a possible spin-Peierls transition at low temperature, whereas a strong antiferromagnetic coupling is observed for **2** along with a possible gradual structural transition at $\sim$220 K.

5. Supplementary material

Crystallographic data for the structural analysis have been deposited with the Cambridge Crystallographic Data Centre, CCDC No. 194817 for **1** and 194818 for **2**. Copies of this information may be obtained free of charge from The Director, CCDC, 12 Union Road, Cambridge, CB2 1EZ, UK (fax: +44-1223-336033; e-mail: deposit@ccdc.cam.ac.uk or www: http://www.ccdc.cam.ac.uk).

Acknowledgements

This work was partially supported by DGI-Spain (Project BQU2000-1157), DGR Catalonia (Project 2001SGR00362) and FCT-Portugal (Contract POCTI/35342/QUI/2000). The collaboration between the team authors from Barcelona and Sacavém was supported by the ICCTI-CSIC bilateral agreement and benefited also from COST action D14.

References

[1] (a) C. Rovira, Chem. Eur. J. 6 (2000) 1723;
(b) C. Rovira, J. Veciana, E. Ribera, J. Tarrés, E. Canadell, R. Rousseau, M. Mas, E. Molins, M. Almeida, R.T. Henriques, J. Morgado, J.-P. Schoeffel, J.-P. Pouget, Angew. Chem., Int. Ed. Engl. 36 (1997) 2323.
[2] (a) E. Dagotto, T.M. Rice, Science 271 (1996) 618;
(b) Z. Hiroi, M. Takano, Nature 337 (1995) 41;
(c) D.J. Scalapino, Science 337 (1995) 12;
(d) E. Dagotto, J. Riera, D.J. Scalapino, Phys. Rev. B 45 (1992) 5744;
(e) S. Gopalan, T.M. Rice, M. Sigrist, Phys. Rev. B 49 (1994) 8901;
(f) C.A. Hayward, D. Poilblanc, L.P. Lévy, Phys. Rev. Lett. 75 (1995) 926.
[3] (a) C. Rovira, J. Veciana, N. Santaló, J. Tarrés, J. Cirujeda, E. Molins, J. Llorca, E. Espinosa, J. Org. Chem. 59 (1994) 3307;
(b) L.-Y. Chiang, P. Shu, D. Holt, D.O. Cowan, J. Org. Chem. 48 (1983) 4713.
[4] J.P. Fackler, D. Coucouvanis, J. Am. Chem. Soc. 88 (1966) 3913.
[5] F.A. Cotton, J.A. McCleverty, Inorg. Chem. 6 (1967) 229.
[6] E.B. Lopes, ITN Internal Report (1991).
[7] P.M. Chaikin, J.F. Kwak, Rev. Sci. Instrum. 46 (1975) 218.
[8] P.E. Schaffer, F. Wudl, G.A. Tomas, J.P. Ferraris, D.O. Cowen, Solid State Commun. 14 (1974) 347.
[9] E.B. Lopes, H. Alves, E. Ribera, M. Mas-Torrent, P. Auban-Senzier, E. Canadell, R.T. Henriques, M. Almeida, E. Molins, J. Veciana, Eur. Phys. J. B 29 (2002) 27.
[10] F. Creuzet, Ph. D. Thesis, Orsay,1981.
[11] Q. Liu, S. Ravy, J.-P. Pouget, C. Coulon, C. Bourbonnais, Synth. Met. 55-57 (1993) 1840.